ingegneria sismica
International Journal of Earthquake Engineering
Anno XLIII - Num. 2 - 2026

Brain-computer interface research on the visualization and analysis of sports rehabilitation training systems supported by artificial intelligence

Yun Jiang[1] *and Peng Huang*[2,*]

[1] Police Practical Combat College of Guangxi Police College, Nanning, Guangxi, 530000, China

[2] Guangxi Health Science College, Nanning, Guangxi, 530000, China

SUMMARY: *In the study, the EEG signals are firstly acquired and processed, and then a multidomain fusion feature extraction algorithm is proposed, which fuses two algorithms, Improved Localized Feature Scale Decomposition (ILCD) and Adaptive Common Spatial Patterns (ACSP), to extract the features of both time-frequency and spatial domains. In order to improve the classification ability of MI signals, a convolutional neural network model based on spatial self-attention and multi-timescale feature extraction is designed to realize the classification of MI signals under motion by introducing multi-scale feature extraction and attention mechanism. Finally, a rehabilitation training system based on the algorithm of this paper was designed using mixed programming in Matlab and C. Subjects were selected for validation. The experimental results show that in the actual experiments with several subjects, the classification accuracy of this paper's algorithm is up to 82%, and the average classification accuracy is 62.19%, and the rehabilitation training system built by the research can accurately extract the user's EEG signals in real time and accurately control the movement of the rehabilitation robot according to the user's imagination.*

KEYWORDS: *brain-computer interface; motor rehabilitation; multi-timescale feature extraction; EEG signal; online system*

1 Introduction

Sports injuries are a common challenge in athletes' careers, and the science and effectiveness of rehabilitation are directly related to the comeback effect and competitive performance of athletes [1]. Due to the intense use of the athlete's body, the injuries suffered by athletes are often more complex and require a longer recovery time than the general population [2]. Therefore, the development of a targeted rehabilitation program is essential to accelerate recovery and reduce the probability of recurrence [3]. Brain-computer interface (BCI) technology, as a novel human-computer interaction technology, translates the brain's intentions into machine actions or commands, bypassing the traditional peripheral nerve and muscle output pathways of the brain, and allowing the brain to communicate and control directly with electronic devices such as computers [4-6]. As a product of the multidisciplinary integration of information science, neuroscience and artificial intelligence, BCI technology is making a significant impact in the fields of neurorehabilitation and human-computer interaction [7]. In the field of rehabilitation training, BCI technology shows great potential for application with its unique advantages.

*18977119455@163.com
https://doi.org/10.65102/is2026511 Published: 30 April, 2026

BCI is an important breakthrough in the field of brain science research in recent years, and has been applied in many fields such as depression, drug addiction, emotional cognitive disorders and physical rehabilitation. In the latest research on exercise rehabilitation training, researchers have established different forms of BCI-based rehabilitation training systems according to the neuroplasticity of patients and the specificity of neurophysiological activities in the motor function areas of the brain, which promote the neural function compensation of patients through specific intensive training, thus helping patients to recover motor and other functions [8-10]. Regarding the current state of research on BCI technology in sports rehabilitation training systems, Liu et al. designed a whole set of sports rehabilitation process based on BCI system, which integrates a variety of rehabilitation modalities, such as high-intensity immersive virtual reality training, rich visual-haptic feedback, and assisted walking training controlled by electroencephalograms [11]. Webb et al. developed a convenient upper extremity exoskeleton BCI system, designed a mechanism to assist in the motor rehabilitation of elbow and forearm joints, using a consumer-grade wireless EEG cap EPOC to read the brain motor imagery data as a means to drive the mechanism action, thus assisting the patient in arm rehabilitation training [12]. Guo, N et al. proposed a steady-state visual evoked potentials-based BCI control system for rehabilitation training, which analyzes the patient's EEG signals to detect the user's intention for the controlling a soft robotic glove for hand function rehabilitation training after stroke [13]. Nann et al. developed a BCI control system for a full arm exoskeleton, which is capable of acquiring and parsing the patient's ocular and EEG signals to control the exoskeleton robotic arm to assist the patient in performing complex tasks, and also provides a new motor rehabilitation training solution for the recovery of the patient's upper limb function [14]. Bhagat et al. implemented a closed-loop upper limb rehabilitation system through BCI and exoskeleton technology, which triggered the movement of the upper limb exoskeleton by inferring the movement intention through the extraction of MRCP features and provided immediate haptic feedback to guide the movement and encourage the user to actively participate [15].

In addition, Costa et al. developed a BCI rehabilitation training system based on three types of MI tasks. This system can parse the three motor intentions of the patient when imagining palmar grasping, pinching, and elbow flexion tasks, thus controlling the corresponding movements of the robotic arm and assisting the patient in motor rehabilitation [16]. Angerhöfer et al. investigated how to integrate a BCI-based motor rehabilitation training treatment program into different stages of neurorehabilitation therapy, and they found that starting immediately after early rehabilitation using BCI-based neurofeedback for treatment is the most appropriate [17]. Kern et al, used BCI technology for rehabilitation therapy, whereby EEG signals from the sensorimotor cortex were converted by BCI into robotic control signals, which were used to control a robotic orthotic to manipulate the patient's paralyzed hand for motor rehabilitation [18]. Mekbib et al. devised a VR (Virtual Reality Technology)- BCI system for the rehabilitation of 10 healthy individuals, and then the virtual reality group showed statistically significant improvement over the control group in terms of upper limb activity performance as assessed by the Motor Function Evaluation Scale (WMF) [19]. Choi et al. proposed a real-time BCI-based lower limb exoskeleton control system, which works by decoding gait and seated motor imagery EEG signals and translating them into the control commands for the exoskeleton system, while using EEG signals during blinking as a switch for system activation [20].

Aiming at the current signal parsing algorithms with low recognition accuracy, difficulty in multi-classification and low real-time performance, this paper proposes a multi-domain fusion EEG signal parsing algorithm, which realizes real-time parsing of users' motor imagery signals. First, the motor imagery EEG signals are collected and preprocessed to remove baseline drift and interference. Then, two algorithms, improved local feature scale decomposition and

adaptive co-space mode, are fused, and the ILCD algorithm is used to decompose the signals, compute the time-frequency energy features, and constitute the time-frequency domain feature vector sets, and the ACSP algorithm is used to construct the spatial filter and extract the spatial domain feature vector sets. Then, the extracted spatial and time-frequency domain features are fused, and a convolutional neural network classifier based on spatial self-attention and multi-timescale feature extraction is proposed to classify and recognize motor imagery EEG signals. Finally, a sports training and rehabilitation system is designed based on the EEG signal parsing method, and finally, subjects are arranged to conduct rehabilitation training experiments to explore the feasibility of the constructed system.

2 Acquisition and Analysis of EEG Signals for Sports Imagery

2.1 EEG signal acquisition and preprocessing

2.1.1 EEG signal acquisition

In order to collect the EEG signals of patients in real time, effectively and accurately, it is very important to select appropriate acquisition equipment through reasonable acquisition methods.

To summarize, there are two main ways to acquire EEG: (1) implantable electrode acquisition; (2) scalp surface electrode acquisition. Both methods are currently used, but implantable electrode acquisition requires craniotomy, which needs to take into account the human body's rejection, and most importantly, it is not suitable for stroke patients to undergo rehabilitation training, which is not in line with the rehabilitation wishes of physicians and patients. Therefore, scalp surface electrode acquisition is generally used to obtain EEG signals.

2.1.2 EEG signal preprocessing

1. Remove baseline drift

There are many methods for baseline drift correction, and the commonly used ones mainly include the following methods: sliding average method, least squares method and median filtering method. Compared with the latter two methods, the sliding average method has obvious advantages: it is convenient and fast, has good real-time performance, and is able to perform complete operations on the data. Based on this, this paper chooses to use the sliding average method to remove the baseline drift in the EEG signal. The specific method is as follows:

First, choose the appropriate window size for the data to be processed, and within the window range, there will be abnormal data values, which need to be processed, and what needs to be done here is to take the average value. Then, move the window operation, and repeat the average calculation, until all the data to be processed to complete the calculation.

Select a segment of data $y(i), i = 0,1,\cdots,n$, set the length of the window to N $(N < n/2)$, and perform an averaging operation on the data within the window $y(0) \sim y(N)$ to obtain $y_1(0)$. Then, set p as the step size and continue to move the window so as to obtain the anomalous value of the center point for curve fitting to obtain $y_1(l), l = 0,1,\cdots,m$. The moving step p and the length m of the fitted curve data obtained from the above have a certain relationship, i.e., $l = (n-N)/p$, and a rounding operation is performed. Finally, the fitted curve is upsampled to obtain $y_1(i), i = 0,1,\cdots,n$.

The preprocessed signal can be obtained by subtracting the original data values from the

anomalous fitted curve values:

$$y_m(i) = y(i) - y_1(i), i = 0,1,\cdots,n \tag{1}$$

2. Remove the industrial frequency interference

In this paper, an adaptive 50Hz filter is used to filter out the IF interference in the EEG signal. The key is to dynamically estimate the artifacts in the input signal by making a difference between the observed signal containing artifacts and the reference artifacts, and then processing and analyzing them based on the criterion of minimum mean square error.

In order to achieve a better filtering effect, it is necessary to realize that the coefficients of the filter can be automatically adjusted accordingly, so that the artifacts can be filtered out to the maximum extent, so that the useful signals can be retained. The design principle of the adaptive filter is shown in Figure 1.

From Figure 1, the output $y(i)$ of the adaptive filter is:

$$y(i) = w(i)^T x(i) \tag{2}$$

The desired output signal $\varepsilon(i)$ is:

$$\varepsilon(i) = s(i) - y(i) \tag{3}$$

The iterative formula for its weight coefficients is:

$$w(i+1) = w(i) + \beta\varepsilon(i)x(i) \tag{4}$$

where β is the global step size.

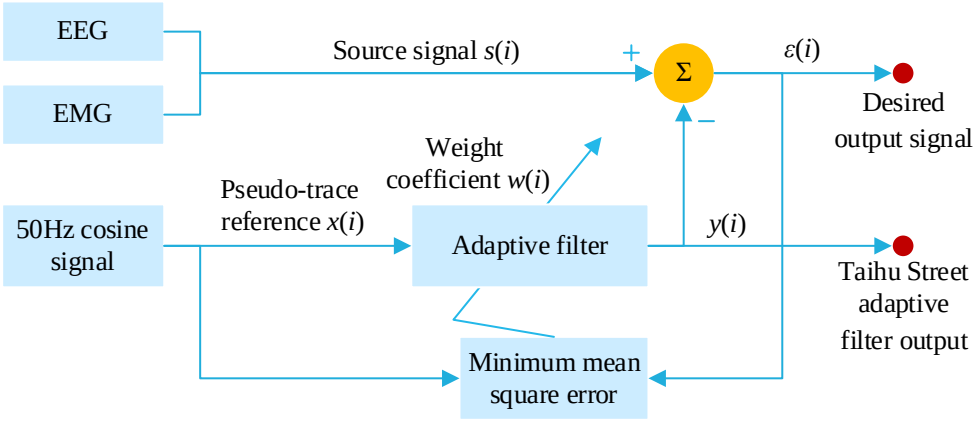

Figure 1: Diagram of adaptive filter

3.Removing oculo-electrical interference in EEG

In the process of EEG acquisition, because the subject will have the behavior of blinking, and this action will produce ocular artifacts interference, which will affect the experimental effect to a certain extent. The system described in this paper uses the Independent Component Analysis (ICA) method to filter out oculo-electrical artifact interference, which is a blind source separation algorithm. The method gained acceptance in the mid-1990s, and studies have shown that ocular artifacts in EEG signals can be effectively removed by the independent component

analysis method.

The block diagram of the ICA algorithm is shown in Figure 2: Let the observed N-dimensional signal be $X(t)=[x_1(t),x_2(t),...,x_n(t)]$, and $S(t)=[s_1(t),s_2(t),...,s_m(t)]$ is the M-dimensional source signal, where the source signal $S(t)$ can be mixed by an unknown matrix A to form the signal $X(t)$ to be observed, i.e., $X(t)=A*S(t)$. Solving the separation matrix W is the core idea of the method, which aims to expect the output signal $U(t)=W*X(t)$ to be as identical as possible to the source signal $S(t)$. And the optimal separation matrix is the separation matrix W that maximizes the non-Gaussianity of the desired output signal $U(t)$ after the separation is performed.

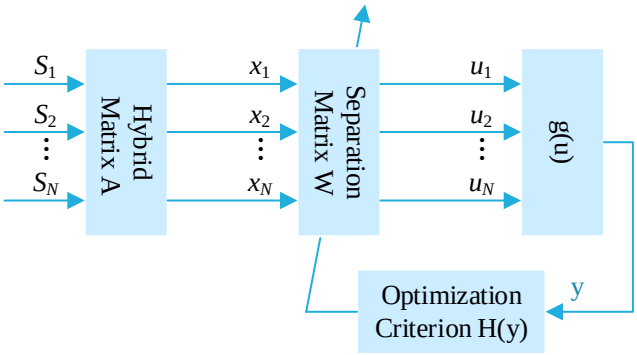

Figure 2: ICA algorithm flow chart

2.2 ILCD-ACSP based motion imagery feature extraction

2.2.1 Improved localized feature scale decomposition method

In this section, the LCD method is improved in terms of mean curve construction by using mean point extension at endpoints and hybrid interpolation. The classical LCD method uses (τ_{k+1},Y_{k+1}) at a certain extreme point and two adjacent extreme points (τ_k,Y_k), (τ_{k+2},Y_{k+2}) in the construction of the local mean curve for estimating the mean point (τ_{k+1},D_{k+1}). However, at the endpoints, the estimation of the mean point has a large deviation of the predicted value from the actual value due to the one-sided extension, which has a large effect on the ISC component at the endpoints. Based on the above considerations, a two-way delay strategy is adopted. Therefore the specific improvements of the LCD algorithm are as follows:

(1) The original signal $x(t)$ is bilaterally delayed by Eq. (5):

$$\begin{cases} Y_0 = Y_2 \\ \tau_0 = 2\tau_1 - \tau_2 \end{cases} \quad \begin{cases} Y_{N+1} = Y_{N-1} \\ \tau_{N+1} = 2\tau_N - \tau_{N-1} \end{cases} \tag{5}$$

The value of the extreme point function of the delayed signal is Y_k and the corresponding moment is τ_k, where $k=1,2,...N-2$.

(2) Take the extreme points $Y(\tau_{k-1})$, $Y(\tau_k)$, $Y(\tau_{k+1})$, and $Y(\tau_{k+3})$.

(3) Compute the localized envelope curves $\eta(t)$, $t \in [\tau_{k-1}, \tau_{k+3}]$, and $\eta(t)$ constrained by the segmented cubic spline fitting method:

$$\begin{cases} \eta(\tau_{k-1}) = Y(\tau_{k-1}) \\ \eta(\tau_{k+1}) = Y(\tau_{k+1}) \\ \eta(\tau_{k+3}) = Y(\tau_{k+3}) \end{cases} \begin{cases} \eta'(\tau_{k-1}) = x'(\tau_{k-1}) \\ \eta'(\tau_{k+1}) = x'(\tau_{k+1}) \\ \eta'(\tau_{k+3}) = x'(\tau_{k+3}) \end{cases} \begin{cases} \eta''(\tau_{k-1}) = x''(\tau_{k-1}) \\ \eta''(\tau_{k+1}) = x''(\tau_{k+1}) \\ \eta''(\tau_{k+3}) = x''(\tau_{k+3}) \end{cases} \tag{6}$$

$$\eta(t) \geq x(t) \; Or \;\; \eta(t) \leq x(t), t \in [\tau_{k-1}, \tau_{k+3}] \tag{7}$$

In the above constraints, Eq. (6) ensures the local smoothness of the envelope curve segments, and Eq. (7) ensures that the amplitude of the local envelope curve, the lower envelope, covers the original signal amplitude.

(4) The signal is divided into a left interval $(k = 1, 2)$, a middle interval $(k = 3, 5, ..., N-2)$ and the right interval $(k = N-1, N)$. Calculate the sequence of local mean points at the moment of the middle interval τ_k according to equation (8):

$$D(\tau_k) = \frac{Y(\tau_k) + \eta(\tau_k)}{2} \tag{8}$$

(5) For the endpoints of the left and right intervals, D_f and D_b denote the mean points obtained by forward and backward interpolation, respectively, and the local mean points at the endpoints are calculated according to equation (9):

$$D(\tau_k) = \begin{cases} D_b(\tau_k), & k = 1, 2 \\ D_f(\tau_k), & k = N-1, N \end{cases} \tag{9}$$

(6) The local mean curve $H(t)$ is computed by fitting all local mean points using cubic spline, and the remaining steps follow the iterative process of the standard LCD method for time-frequency decomposition.

2.2.2 Adaptive co-spatial modeling approach

The co-spatial pattern algorithm is a commonly used algorithm for spatial domain feature extraction, which is capable of extracting null domain features from spatial filtering of EEG signals. The basic principle of the algorithm is to simultaneously diagonalize the covariance matrices from different signal classes, and then find a spatial filter with the strongest discriminative properties for projection, so that the two classes of signals to be classified can be maximally distinguished. The specific method is as follows:

The $N \times T$ -dimensional matrices E_1 and E_2 are the EEG data of the two types of motor imagery task experiments, N is the number of EEG channels and T is the number of sampling points, respectively. The normalized covariance matrices C_1 and C_2 are shown in Eq. (10) respectively:

$$C_1 = \frac{E_1 E_1^T}{trace(E_1 E_1^T)}, C_2 = \frac{E_2 E_2^T}{trace(E_2 E_2^T)} \tag{10}$$

In the above equation, E_1^T denotes the transpose of the E_1 matrix, and $trace(E)$ denotes the sum of the elements on the diagonal of the matrix, i.e., the trace of E of the matrix.

The mixed space covariance matrix C is shown in equation (11):

$$C = C_1 + C_2 \tag{11}$$

The eigenvalue decomposition of the mixed-space covariance matrix C is performed according to equation (12):

$$C = U \lambda U^T \tag{12}$$

In the above equation, U denotes the eigenvector of matrix C and λ is the corresponding eigenvalue.

Calculate the whitening value matrix:

$$P = \lambda^{-\frac{1}{2}} U^T \tag{13}$$

Transform C_1 and C_2 into S_1 and S_2 using the whitening matrix:

$$\begin{aligned} S_1 &= P C_1 P^T = B \Sigma B^T \\ S_2 &= P C_2 P^T = B(I - \Sigma) B^T \end{aligned} \tag{14}$$

where Σ_1 and Σ_2 are eigenvalue diagonal arrays and B is the eigenvector matrix common to S_1 and S_2.

Construct the spatial filter corresponding to the projection matrix W:

$$W = U^T P \tag{15}$$

The EEG data $x(t)$ from the original motor imagery task experiment can be passed through W to obtain the new data Z_0:

$$Z_0 = x(t) \cdot W \tag{16}$$

Construct the matrix $Z = [z_1, z_2, \cdots, z_{2m}] \in R^{N \times 2m}$ consisting of the first $m (m < T/2)$ rows and the last m rows of Z_0, and the eigenvectors $f = [f_1, f_2, \cdots, f_{2m}] \in R^{2m \times 1}$ which are defined as:

$$f = \frac{\mathrm{var}(z_i)}{\sum_{j=1}^{2m} var(z_j)} (i = 1, 2, \cdots, 2m) \tag{17}$$

Traditional CSP feature extraction uses fixed covariances that come from training set data. Instead, we apply an adaptive idea and use an adaptive co-space pattern (ACSP) to increase the generalization ability of the algorithm. In ACSP feature extraction, when a new trial is encountered or for a certain EEG segment (e.g., $x(k)$), we update the corresponding covariance matrix as follows:

$$C(k) = \mu C(k-1) + (1-\mu) x(k) x^T(k) \tag{18}$$

where $\mu \in [0,1]$ is the update coefficient.

This adaptive strategy embodies the idea of weighted averaging. The updated covariance matrix is equal to the weighted sum of the historical covariance matrix and the current record segment covariance matrix. For equation (18) above, both covariance components on the right side of the equation are necessary. $C(k-1)$ contains the historical information, which allows the signal features to be passed on and helps to improve the robustness of the new covariance matrix $C(k)$ after updating. The updated covariance matrix contains the newly added information, which can reflect the time-varying characteristics of the EEG signal.

2.2.3 OVR-ACSP

In this paper, we apply the OVR idea to the ACSP feature extraction algorithm mentioned above. To be precise, if four sets of EEG experimental data corresponding to four different tasks A, B, C, and D are given, we use each set of data to obtain the covariance matrices C_A, C_B, C_C, and C_D, respectively. Then the covariance matrix C_{A_Rest} is obtained by combining the data samples from the classification tasks B, C, and D. Similarly, the covariance matrices C_{B_Rest}, C_{C_Rest}, and C_{D_Rest} can be obtained. Next we perform the above ACSP procedure using each pair of covariance matrices (e.g., C_A and C_{A_Rest}), which can be extended to the multiclassification problem.

2.2.4 Feature fusion

The time-frequency domain feature vector set F_1 obtained by the improved local feature scale decomposition method and the spatial domain feature vector set F_2 obtained by the adaptive co-space pattern method in this chapter are connected together using the serial feature fusion strategy, in which the multiple features are first normalized, and then linked together head-to-tail, with the specific forms as follows:

$$\begin{cases} F_1 = \left[\dfrac{E_{11}}{\|E_{11}\|}, \cdots, \dfrac{E_{13}}{\|E_{13}\|}, \cdots, \dfrac{E_{43}}{\|E_{43}\|} \right] \\ F_2 = \left[\dfrac{f_1}{\|f_1\|}, \dfrac{f_2}{\|f_2\|}, \dfrac{f_3}{\|f_3\|}, \dfrac{f_4}{\|f_4\|} \right] \\ F = [F_1, F_2] \end{cases} \tag{19}$$

2.3 Conductor Selection

In this chapter, the co-space model is considered as an algorithm for spatial filtering, and the resulting projection matrix W contains the spatial information of each lead. By calculating the contribution rate of each lead, a number of channels with larger weight values are selected for lead optimization as follows:

(1) For spatial filtering using the CSP method described in the previous subsection, where $x(t)$ is the raw EEG data and $W \in R^{N \times N}$ is the spatial filter, which is specified as:

$$Z_0 = x(t) \cdot W = \begin{bmatrix} x_1 \\ \vdots \\ x_N \end{bmatrix} \begin{bmatrix} \omega_{11} & \cdots & \omega_{1N} \\ \vdots & \ddots & \vdots \\ \omega_{N1} & \cdots & \omega_{NN} \end{bmatrix} \tag{20}$$

(2) Let $W = [w_1, w_2, \cdots, w_N]$, where $w_i (i = 1, 2, \cdots, N)$ refers to the ith column vector in the spatial filter W, and w_i stands for the weight value of the signal $x_i (i = 1, 2, \cdots, N)$ of the individual leads in the projected space, which embodies the weights of the different leads after the spatial filtering on the original signal $x(t)$. This effect is further quantified by calculating its contribution $RC(i)$ for each lead using the form of Euclidean paradigm:

$$RC(i) = \frac{\|w_i\|_2}{\|W\|_2} \tag{21}$$

The $\|\cdot\|_2$ in the above equation refers to the Euclidean paradigm for this vector or matrix. The larger value of $RC(i)$ indicates that this derivative contains more valid information and has more influence on the signal Z_0 after spatial projection, in contrast, the smaller value of $RC(i)$ indicates that there is less valid information and less influence of Z_0.

(3) Using the above equation (21), the contribution rate $RC(i)$ of each lead is calculated and sorted according to the value from high to low, and the M ones with the highest $RC(i)$ are selected as the optimized lead group to obtain the new spatially filtered signal Z':

$$Z' = x'(t) \cdot W' = \begin{bmatrix} x_1 \\ \vdots \\ x_M \end{bmatrix} \begin{bmatrix} \omega_{1M} & \cdots & \omega_{1M} \\ \vdots & \ddots & \vdots \\ \omega_{M1} & \cdots & \omega_{MM} \end{bmatrix} \tag{22}$$

2.4 MI signal classification based on SAMS-CNN network

2.4.1 Network modeling

In order to improve the decoding and classification ability of MI signals, a convolutional neural network based on spatial self-attention and multi-timescale feature extraction is designed in this section, and the network mainly contains three modules: the spatial self-attention module, the multi-timescale feature extraction module and the feature fusion classification module. The details are shown in Fig. 3.

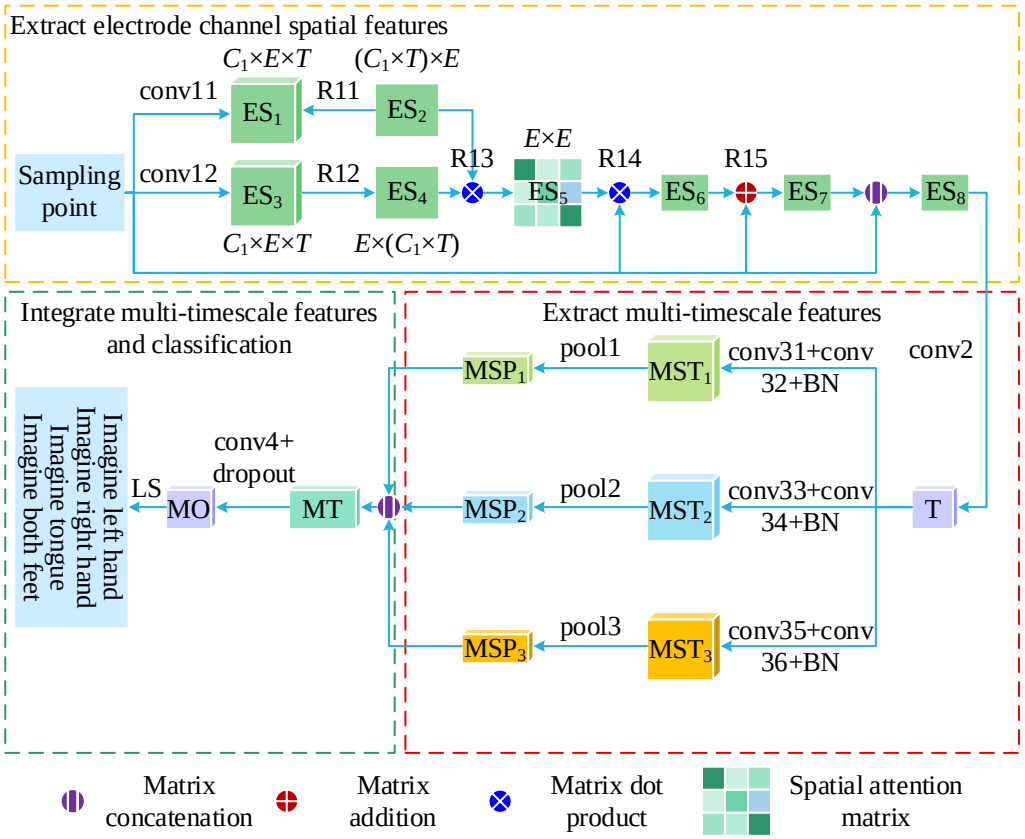

Figure 3: Network model structure diagram

2.4.2 Training strategies

The EAMS-CNN network model is implemented based on pytorch deep learning architecture. In order to increase the computational power and reduce the time for model training, a high performance server with GPU NVIDIA 2080Ti is used for training the algorithm model in this experiment. Negative log-likelihood is chosen for the loss function, and the formula is shown in (23):

$$LOSS(\theta) = -\frac{1}{N}\sum_{i=1}^{N} y_i \cdot \log\left(p(y_i)\right) \tag{23}$$

where N is the total number of MI tasks, y denotes the true label, and $p(y)$ denotes the predicted label probability. During the training process, the weights of the neural network are updated by back propagation, considering the non-stationarity of the input signal and the relative simplicity of the network model, this experiment uses the Adam optimizer to optimize

the network, with the learning rate and the decay weights set to 0.0001 and 0.01, respectively. the batch size is set to 64, and all the parameter initialization operations in the model are implemented by the Xavier algorithm. The BCI1V2a dataset itself has been divided into a training set and a test set, in this chapter of work we keep the test set unchanged and divide the training set in a randomized manner into a training set and a validation set in the ratio of 8:2, which are used for training the model.

The model training process also employs an early-stop strategy widely used in semantic segmentation, etc., which consists of two phases: in the first phase, only the training set is subjected to the training operation (i.e., backpropagation to update the weights) and when the accuracy of the validation set is no longer improved within the preset Epoch value (set to 600 in this experiment), the training in the first phase is completed and the first phase's optimal network model is saved parameters to be used as the initial values of the network model parameters in the second phase. In the second stage, the training operation is continued by merging the training and validation sets until the Loss on the test set decreases to the optimal Loss on the validation set in the first stage, and the whole training process ends.

3 Experimental results and discussion

3.1 EEG data and processing

Data sets 2a from the 4th BCI competition were used, provided by the University of Graz. Twenty-two Ag/AgCl electrodes were used to record EEG signals on the scalp. The dataset consisted of four imagined movements of the left hand, the right hand, both feet and the tongue. 10 subjects recorded the EEG signal datasets on two separate days. Each data set consisted of six separate data strings separated by a rest period. Each data string consisted of 50 experiments, with 12 experiments for each type of imagery movement. Thus a data set has 300 experiments.

For the experiments, subjects sat in front of a computer and followed the computer prompts. An experiment lasted 8 seconds. At t=0, a cross is displayed on a black screen, and a short sound reminds the subject that the experiment is starting. At t=2s, an arrow up, down, left, or right (corresponding to tongue, biped, left hand, and right hand, respectively) prompted the subject to visualize the task. At t=3.25s, the arrow disappears. There was no feedback during the process, and subjects had to perform motor imagery until the cross disappeared at t=6s.

During the experiment, the electrodes were sampled at a rate of 260hz and the signal was processed using a bandpass filter from 0.5hz to 100hz and a trap filter at 50hz. The dataset for each subject can be divided into two parts, the dataset Train and Evaluation, which include 300 experiments respectively.

In order to remove artifactual interference and improve the signal-to-noise ratio of the signal, the EEG signal needs to be filtered first before extracting the features. In this chapter, the data in the dataset were filtered at 8-30 Hz to remove the interference according to the characteristics of ERD and ERS. The data of 2.5s-3.5s were selected for classification and processing, and the signals before and after filtering are shown in Fig. 4, and the signals fluctuated relatively little in the range of 0-260hz after the processing was carried out.

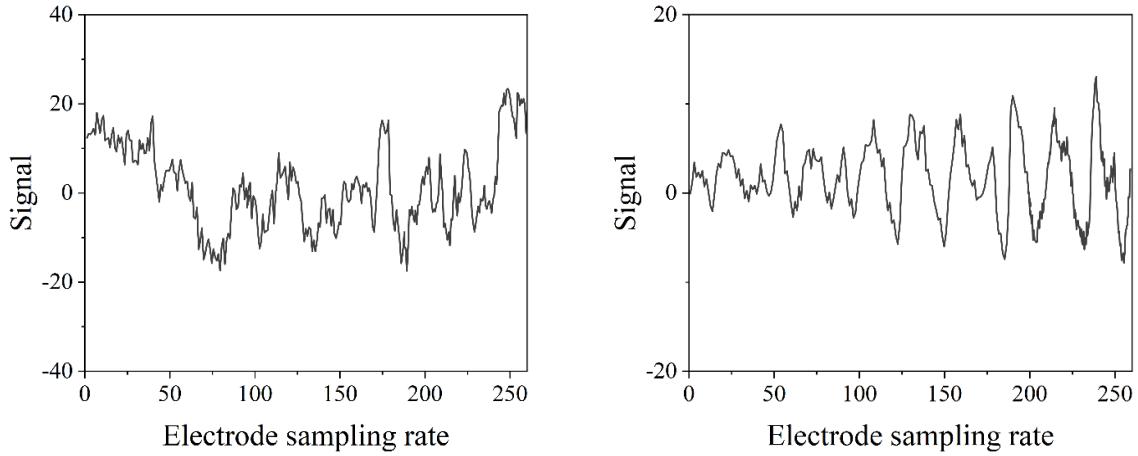

(a)260 original data points (b)260-point filtered data

Figure 4: C3 channel EEG signal images before and after filtering

To address the problems of large ILCD computation and high dimensionality after feature fusion, this chapter only selects the three channels C3, C4 and Cz with the largest contribution from the 22-conducted signals, and performs ILCD time-frequency decomposition on them, and decomposes each channel to obtain three ISC components, which makes a total of nine ISC components, and extracts frequency domain features F1 from the nine ISC components according to the method above.Fig. 5 is the graph of ISC component after ILCD decomposition of the EEG signal of the C3 channel in an experiment. Figure 5 shows the ISC component diagram of the EEG signal of C3 channel after ILCD decomposition.

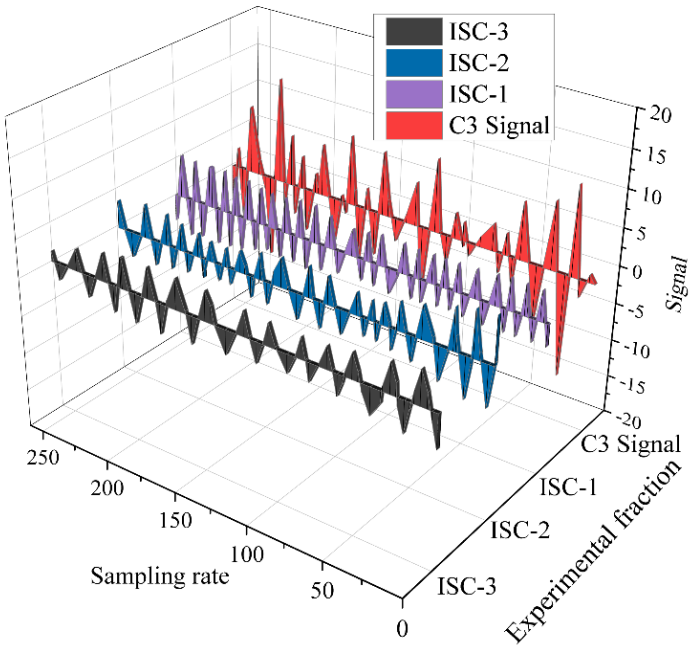

Figure 5: The ISC component graph after ILCD decomposition

The original 22-conductor EEG signal and 9 ISC components are integrated, followed by spatial feature and time-frequency domain feature extraction for this integrated signal. Finally, the two feature vectors F_1 and F_2 are fused into the feature F. F is sorted by MCFS and input

into the SAMS-CNN classifier for training and testing.

3.2 Experimental results and analysis

The algorithms proposed in this paper are compared with the Discrete Wavelet Transform DWT (DWT) as well as the fusion of Power Spectral Density + Autoregressive Parameters and Hjorth Parameters to improve the classification of EEG signals (PSD+AR+Hjorth). In addition, 22-channel ACSP algorithm, and 31-channel ACSP algorithm are implemented in this chapter. Among them, 22-channel ACSP is the ACSP processing of only the original 22-channel EEG signals.31-channel includes the acquired 22-channel motor imagery EEG signals and the 9 ISC components obtained from the decomposition of C3, C4, and Cz by the ILCD.31-channel ACSP algorithm is the null-domain feature extraction of the appealing 31 signal data.

Keeping the operating parameter $2m$ =8 constant and using the same classifier, this section compares the classification performance of these five algorithms as shown in Table 1. Each figure in the table represents the classification accuracy for four types of motor imagery tasks for that subject. These four types of motor imagery tasks are left-handed, right-handed, bipedal, and tongue.

In the table, the 31-channel ACSP algorithm improved the average classification accuracy for 9 subjects compared to the 22-channel ACSP algorithm. This demonstrates the importance of the nine ISC components generated by the ILCD decomposition in the classification of EEG signals. By comparing with the 22-channel ACSP and 31-channel ACSP algorithms without time-frequency domain features, the algorithm proposed in this chapter has the best average performance, and the highest accuracy of this paper's algorithm is 82% and the average accuracy is 61.38% in 9 subjects, which demonstrates the effectiveness of time-frequency domain features extracted by the algorithm in this chapter.

Table 1: Classification accuracy of motor imagery EEG data in 9 subjects(%)

Subjects	DWT	PSD+AR+Hjorth	22 channel ACSP	31 channel ACSP	SAMS-CNN
1	56.3	56.7	63.3	66.4	64.7
2	34.1	37.9	37.2	42.4	42.8
3	60.8	51.1	79.6	77.5	77.8
4	41.4	44.2	55.6	60.1	59.8
5	34.1	33.1	37.6	36.9	36.9
6	44.5	42.4	40.0	44.5	43.8
7	42.8	51.1	65.3	65	67.1
8	59.8	51.8	75.8	76.1	77.5
9	60.1	65.0	79.6	78.5	82.0
Mean	48.21	48.14	59.33	60.82	61.38

To further illustrate the effectiveness of the algorithms in this chapter, the average classification correctness of the algorithms in this chapter under different $2m$ was compared with the 22-channel ACSP and the 31-channel ACSP, as shown in Table 2. Each data in the table is the average correct classification rate of 9 subjects under different $2m$ parameters.

The analysis shows that for most values of 2m, the classification algorithm proposed in this paper obtains the best classification results with an average accuracy of 62.19% under the same experimental conditions. Moreover, the proposed algorithm improves the classification results of the ACSP algorithm as a whole. This fully reflects the effectiveness of the proposed algorithm in this chapter.The average classification correctness of the 31-channel ACSP algorithm is higher than that of the 22-channel ACSP algorithm, which illustrates the

effectiveness of the ILCD method for the classification of motor imagery EEG signals.

Table 2: The average classification accuracy of 9 subjects under different $2m$ parameters

$2m$	22 channel ACSP	31 channel ACSP	SAMS-CNN
2	59.2	59.6	60.6
4	62.4	62.3	62.9
6	61.2	61.4	62.1
8	60.5	62	62.6
10	60.4	62.2	62.9
11	61.3	62.7	62.4
12	61.2	62.7	62.2
16	60.8	62.1	61.8
18	60.8	61.6	62.3
20	60.5	61.7	62.1
22	60.6	61.3	62.2
Mean	60.81	61.78	62.19

4 Brain-computer interface-based sports rehabilitation training system

4.1 Overall program design of the system

The signal processing part of this system mainly corresponds to the algorithm design of MI-BCI system. In order to facilitate the user's use, this system adds an interface development part to visualize the process and results of EEG signal processing, while the control feedback part mainly corresponds to the modification of the lower limb rehabilitation equipment.

Since the focus of this paper is on the study of the MI-BCI system, only the modification of the mechanical part is briefly introduced. The main body of the lower limb rehabilitation equipment is a DYW-1-LT model electric wheelchair produced by a company. Some performance parameters of this electric wheelchair are shown in Table 3. In order to adapt to the rehabilitation training of the sitting and standing motor function of stroke patients, it is necessary to remodel the sitting board part of the wheelchair and add the ergonomic lifting function.

Table 3: Some Performance Parameters of Electric Wheelchair

Nme	Performance parameter
Pwer of motor	355w*2
Bttery capacity	13Ah
Mximum speed	9km/h
Baking ability	≤1.6km
Net weight	25.3kg

4.1.1 Design of the control part of the system

The control part consists of STM32 control board, battery, motor driver, motor, WiFi to serial module, distance sensor and upper computer, etc. It can be divided into three modules: motor driver, obstacle avoidance control and WiFi communication. The motor drive module is responsible for the power supply and motor drive of the whole lower limb rehabilitation

equipment to control the lifting and lowering of the sitting board and the forward and backward movements of the electric wheelchair. The obstacle avoidance control module monitors the distance between the electric wheelchair and the obstacles in front in real time, and sends out the braking command in time when it encounters obstacles smaller than the safe distance to protect the user's safety.The WiFi communication module realizes the wireless communication between the upper computer (PC) and the lower limb rehabilitation equipment, and converts the output from the algorithm module in the upper computer (PC) into the control signal for controlling the lifting and lowering of the lifting module.

4.1.2 Design of the motor drive module

The motor drive module contains components such as battery, STM32 control board, motor driver, pusher motor and hub motor. The battery is a lithium battery matched with DYW-1-LT type electric wheelchair, whose output rated voltage is 24V and capacity is 10Ah.

The main controller chip model of the STM32 control board is STM32F407VET6, which uses 24V power input and has six on-board serial ports, which can provide 5V or 12V power output after the on-board voltage reduction circuit. Two of the UART serial ports are connected to the ESP8266 module and the HMI serial screen respectively, and the baud rate of the serial port is 115200.

4.1.3 Design of obstacle avoidance control module

The obstacle avoidance control module mainly contains two infrared light distance sensors and two ultrasonic distance sensors in addition to the STM32 control board. The ultrasonic distance sensor, model KS103, with a detection distance of 1~800cm and a detection frequency of 500Hz, is connected to the STM32 control board through the I2C/485 serial port, and is able to automatically respond to the commands of the control board, with a response delay of 80ms or less. The model of infrared distance sensor is E18D80NK, by demodulating the infrared light reflected from the object, it can effectively avoid the interference of visible ambient light, and its effective monitoring distance is 80cm.

4.2 Construction of MI-BCI based rehabilitation training system

4.2.1 Software design of the system

This system is designed based on Matlab 2020a platform, using Matlab and C language mixed compilation. Matlab is not able to directly call the files compiled in C. Matlab provides the MEX tool, which can compile C++ code into files and function interfaces that can be executed by Matlab.C/C++ is a popular high-level language, which can be used to directly manipulate the operating system, hardware, and applications in the operating system, and has its own unique advantages over other interpreted high-level languages. C/C++ is a popular high-level language that can directly operate the operating system, hardware and application software in the operating system, and it has its own unique advantages compared with other interpreted high-level languages.Matlab's advantage lies in matrix operation, and the efficiency of loop operation is not as good as that of C++, so this paper is based on the hybrid programming of Matlab and C to make use of both sides of the advantages, so as to make the system run more efficiently. The structure of the interface design of this paper is shown in Figure 6.

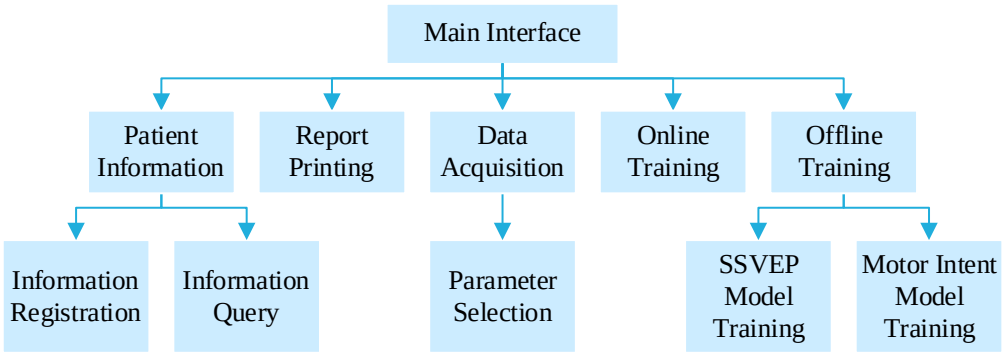

Figure 6: Interface Design Structure Diagram

4.2.2 System hardware equipment design

1. EEG signal acquisition equipment

There are mainly two types of EEG signal acquisition methods, implantable and non-implantable, and the most used is the non-implantable type at present. Non-implantable acquisition mainly includes EEG, functional MRI, and so on. In this paper, the acquisition is EEG, which has the advantages of simple acquisition and cheap price. The EEG acquisition equipment used in this time is through the DSI-24 EEG system of Wearable sensing company, the sensor of this system has the advantages of high impedance and dry contact, and there is no need to fill in the conductive paste during the whole experimental process, and the preparation can be finished in three minutes, which is convenient and comfortable.

2. EEG signal processing equipment

The EEG signal processing equipment is a computer equipped with Matlab, which connects the EEG cap device through the USB port, transmits the data collected by the EEG cap to the DSI-Streamer data acquisition software in real time, and receives the marking information in real time to the data acquisition software through the parallel port marking line, and then the data acquisition software transmits the EEG data and the marking information to the EEG data processing software in real time. Realize the real-time processing of data. After the EEG signals are processed, the computer generates a control instruction code to control the rehabilitation training host, and then the computer sends the instruction code to the rehabilitation training host through Bluetooth.

3. Rehabilitation training drive host and pneumatic gloves

This time, we use Buenkang hand function rehabilitation mainframe, which has the advantages of small size, high portability, low price, secondary development, stable signal reception, low latency, and simple interface operation. The gloves used for rehabilitation training are driven by the air pump in the rehabilitation training mainframe. The gloves are available in different sizes to meet the training needs of all patients.

Host part: There is a Bluetooth module for receiving signals, which can receive Bluetooth control signals from the host computer and drive the pneumatic gloves to move according to the received control signals.

Glove part: mainly drive the hand to carry out the corresponding movement, according to their own needs to choose their own desired training action.

Features: The whole set of equipment is inexpensive, durable, lightweight and so on, which allows patients to continue rehabilitation training after discharge.

4.3 Establishment of the sample data set

Sample dataset establishment this module, the main work is to collect the user's training samples

and organize the collected EEG signals into a sample dataset. The subject's imagining process is also roughly the same as the training process arranging the subject to imagine the corresponding four tasks of tongue, foot, left hand and right hand according to the up, down, left and right arrows, planning to collect 14 rounds of data and 168 sets of motor imagining data.

4.4 Training models

Before model training, the signals in the sample dataset need to be filtered. In the imagination experiments, although a simple filtering and trapping process was set up for the brain-computer interface device, the artifacts need to be further removed in this module because the limitations of the device do not allow free adjustment of the parameters. In this paper, the collected EEG signals were filtered to reject artifacts at 8-30Hz, because the main signals of motor imagery are concentrated in this band. The effect of filtering is shown in Fig. 7, which compares the signal filtering before and after extracting the C3 channel of a certain subject.

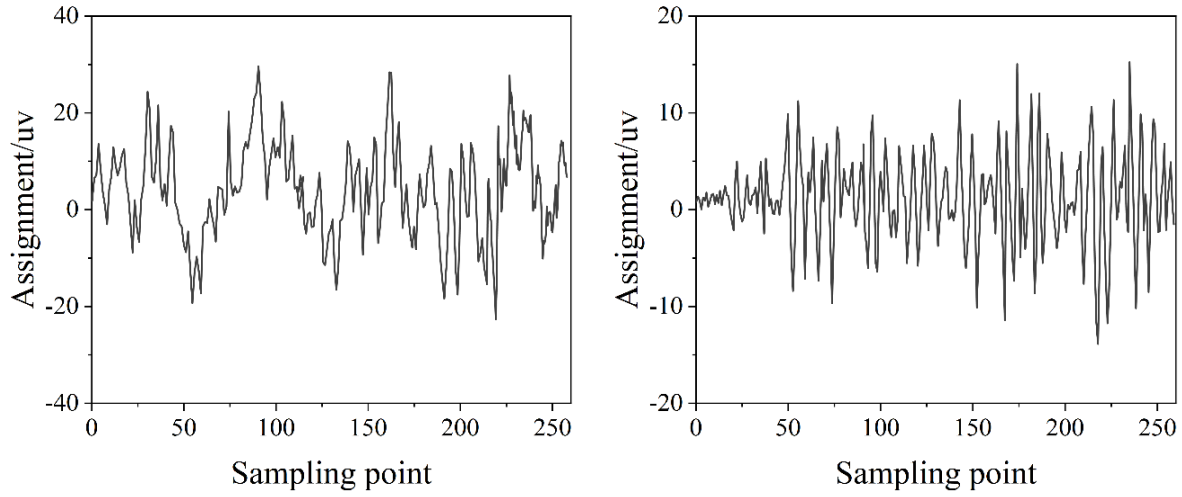

(a)Primitive EEG signals (b)Filtered EEG signal

Figure 7: Comparison of c3 channel signal filtering before and after

4.5 Rehabilitation training experiments

The main work of the Rehabilitation Training Experiment Module is to conduct actual rehabilitation experiments to verify the performance of the rehabilitation system. The module is divided into three steps, which are data acquisition, signal parsing and controlling the robotic arm.

The screen image first displays the cross and lasts for 1.5 seconds, and the subject is prompted to prepare for imagery. Next, a start image popped up on the screen, at which point the subject was free to visualize any one of the four tasks for 4 seconds. At the end of the visualization, the movements of the robotic arm were observed and recorded. Subjects will be tested on 60 sets of data, 15 sets for each task.

After parsing the signals, we need to convert the judged signal categories into control commands and transmit the control commands to the control program of the robotic arm to reach the control of the robotic arm. In this process, we directly convert the judged signal categories into corresponding control commands in the signal parsing program and transmit the commands to the control program of the robotic arm, which will realize the corresponding actions according to the corresponding commands.

These four robotic arm movements respectively correspond to the four types of motor imagination tasks of the subjects. The four motor imagination tasks of imagining the tongue, feet, left hand and right hand respectively correspond to the four movements of "up", "down", "left" and "right" of the robotic arm, thereby achieving the control of the robotic arm. In the experiment, the up, down, left and right indicator arrows displayed on the screen respectively expected the robotic arm to complete the four actions of "up", "down", "left" and "right".

4.6 Practical results and analysis

In order to verify the effectiveness of the MI-BCI-based rehabilitation system, a subject was arranged to actually use the system to verify whether the system was reliable. The subject conducted the experiment according to the experimental flow arranged in the previous subsection. 168 sets of motor imagery signal data were expected to be collected to build the training set, but when collecting one set of imagery data, the subject indicated that there was a serious distraction phenomenon, so the data in that group was excluded, and finally 167 sets of data were obtained to build the training set. After building the algorithmic model according to the training set, 40 sets of actual rehabilitation training test experiments were conducted. At the end of each rehabilitation training action, we will record the actual and desired actions of the robotic arm for each test, and get the test results of the experimental records as shown in Table 4.

According to the performance of the rehabilitation system in the actual experiments, it can be seen that the rehabilitation training system based on motor imagery brain-computer interface that we have established can reach the control of up-down, left-right, and right-right movements of the rehabilitation robot.

According to the table, the average accuracy rate of the electroencephalogram (EEG) signal recognition of the rehabilitation training system we have established has reached 46%. The accuracy rate of discriminating the "left" intention of the user's action has reached 52.5%, the accuracy rate of discriminating the "right" intention of the action is 55%, the accuracy rate of discriminating the "up" intention of the action is 35%, and the accuracy rate of discriminating the "down" intention of the action is 40%. This indicates that during the user's use of the rehabilitation training system, they have achieved good results in controlling the "left" movement, but the control effect on the "down" movement is relatively poor.

Table 4: Rehabilitation Training Experiment Record

Number of experiments	1	2	3	4	5	6	7	8	9	10
Expected action	Left	Right	Right	Left	Up	Down	Left	Right	Up	Down
Actual action	Left	Right	Up	Left	Up	Right	Left	Right	Down	Down
Number of experiments	11	12	13	14	15	16	17	18	19	20
Expected action	Down	Up	Right	Up	Left	Left	Up	Down	Right	Down
Actual action	Down	Up	Right	Up	Left	Left	Right	Down	Right	Down
Number of experiments	21	22	23	24	25	26	27	28	29	30
Expected action	Left	Up	Right	Down	Up	Down	Left	Down	Down	Left
Actual action	Left	Up	Up	Right	Up	Right	Left	Right	Left	Left
Number of experiments	31	32	33	34	35	36	37	38	39	40
Expected action	Up	Left	Down	Right	Up	Right	Down	Left	Right	Up
Actual action	Up	Up	Down	Right	Up	Left	Right	Left	Right	Up

According to the performance of the rehabilitation system in the above practical experiments, it can be seen that the rehabilitation training system based on the brain-computer

interface of motor imagination that we have established can realize the real-time acquisition, preprocessing and parsing of the EEG signals, and can convert the motor imagination signals into real-time inputs to the rehabilitation robot to control the up-down, left-right, and right-right motions of the rehabilitation robot. However, the accuracy of the motion control of the rehabilitation training system is highly correlated with the subject's imagination ability.

5 Conclusion

In this paper, we propose an improved local feature scale decomposition (ILCD) combined with adaptive co-spatial pattern method (ACSP) for ILCD decomposition of partial leads of EEG signals, and decoding classification of MI signals through a convolutional neural network model (SAMS-CNN) based on spatial self-attention and multi-temporal scale feature extraction, and it achieves an average of 62.19% in the classification experiment accuracy in the classification experiment. The online MI-BCI rehabilitation system is built, and the experimental results show that the system can accurately extract and analyze the user's EEG signals in real time and accurately control the movement of the rehabilitation robot according to the user's imagination.

About the Author

Yun Jiang, male, born in 1980, is a lecturer at the Police Combat Training Department of Guangxi Police College. He holds a master's degree in Physical Education and Sports Training from Guangxi University for Nationalities. He is a second-level national martial arts sanda athlete and has been awarded the rank of fifth dan in martial arts. He is also a second-level national referee for martial arts routines, sanda, table tennis, and track and field events. He has led one municipal-level research project and participated in four others. He has published a monograph and over ten papers. After graduation, the author has dedicated over 20 years to the field of physical education. During this time, his research focuses gradually shifted towards the intersection of artificial intelligence and sports rehabilitation. With the rapid advancement of technology, AI has shown great potential in enhancing athletic performance, assisting in rehabilitation training, and preventing sports injuries. Moving forward, the author plans to further explore the application of BCI (Brain-Computer Interface) technology in sports rehabilitation to provide athletes with more precise and efficient rehabilitation methods, helping them better adjust their training pace and intensity.

References

[1] Wang, Z., Zhang, W., & Wang, J. (2022). Muscle injury and sports rehabilitation management in endurance training oriented to winter sports. Revista Brasileira de Medicina do Esporte, 29, e2022_0169.

[2] Ramos, G. A., Arliani, G. G., Astur, D. C., Pochini, A. D. C., Ejnisman, B., & Cohen, M. (2017). Rehabilitation of hamstring muscle injuries: a literature review. Revista brasileira de ortopedia, 52(1), 11-16.

[3] Mackey, A. L., Mikkelsen, U. R., Magnusson, S. P., & Kjaer, M. (2012). Rehabilitation of muscle after injury–the role of anti-inflammatory drugs. Scandinavian journal of medicine & science in sports, 22(4), e8-e14.

[4] Peksa, J., & Mamchur, D. (2023). State-of-the-art on brain-computer interface technology. Sensors, 23(13), 6001.

[5] Karikari, E., & Koshechkin, K. A. (2023). Review on brain-computer interface technologies in healthcare. Biophysical reviews, 15(5), 1351-1358.

[6] McFarland, D. J., & Wolpaw, J. R. (2017). EEG-based brain–computer interfaces. current opinion in Biomedical Engineering, 4, 194-200.

[7] Bockbrader, M. A., Francisco, G., Lee, R., Olson, J., Solinsky, R., & Boninger, M. L. (2018). Brain computer interfaces in rehabilitation medicine. PM&R, 10(9), S233-S243.

[8] Daly, J. J., & Huggins, J. E. (2015). Brain-computer interface: current and emerging rehabilitation applications. Archives of physical medicine and rehabilitation, 96(3), S1-S7.

[9] Orban, M., Elsamanty, M., Guo, K., Zhang, S., & Yang, H. (2022). A review of brain activity and EEG-based brain–computer interfaces for rehabilitation application. Bioengineering, 9(12), 768.

[10] Wang, H., Song, Q., Zhang, L., & Liu, Y. (2012). Design on the control system of a gait rehabilitation training robot based on Brain-Computer Interface and virtual reality technology. International Journal of Advanced Robotic Systems, 9(4), 145.

[11] Liu, J., Abd-El-Barr, M., & Chi, J. H. (2016). Long-term training with a brain-machine interface-based gait protocol induces partial neurological recovery in paraplegic patients. Neurosurgery, 79(6), N13-N14.

[12] Webb, J., Xiao, Z. G., Aschenbrenner, K. P., Herrnstadt, G., & Menon, C. (2012, June). Towards a portable assistive arm exoskeleton for stroke patient rehabilitation controlled through a brain computer interface. In 2012 4th IEEE RAS & EMBS International Conference on Biomedical Robotics and Biomechatronics (BioRob) (pp. 1299-1304). IEEE.

[13] Guo, N., Wang, X., Duanmu, D., Huang, X., Li, X., Fan, Y., ... & Hu, Y. (2022). SSVEP-based brain computer interface controlled soft robotic glove for post-stroke hand function rehabilitation. IEEE transactions on neural systems and rehabilitation engineering, 30, 1737-1744.

[14] Nann, M., Cordella, F., Trigili, E., Lauretti, C., Bravi, M., Miccinilli, S., ... & Soekadar, S. R. (2020). Restoring activities of daily living using an EEG/EOG-controlled semiautonomous and mobile whole-arm exoskeleton in chronic stroke. IEEE Systems Journal, 15(2), 2314-2321.

[15] Bhagat, N. A., Venkatakrishnan, A., Abibullaev, B., Artz, E. J., Yozbatiran, N., Blank, A. A., ... & Contreras-Vidal, J. L. (2016). Design and optimization of an EEG-based brain machine interface (BMI) to an upper-limb exoskeleton for stroke survivors. Frontiers in neuroscience, 10, 122.

[16] Costa, A. P., Møller, J. S., Iversen, H. K., & Puthusserypady, S. (2018, November). Adaptive CSP for user independence in MI-BCI paradigm for upper limb stroke

rehabilitation. In 2018 IEEE Global Conference on Signal and Information Processing (GlobalSIP) (pp. 420-423). IEEE.

[17] Angerhöfer, C., Colucci, A., Vermehren, M., Hömberg, V., & Soekadar, S. R. (2021). Post-stroke rehabilitation of severe upper limb paresis in Germany–toward long-term treatment with brain-computer interfaces. Frontiers in Neurology, 12, 772199.

[18] Kern, K., Vukelić, M., Guggenberger, R., & Gharabaghi, A. (2023). Oscillatory neurofeedback networks and poststroke rehabilitative potential in severely impaired stroke patients. NeuroImage: Clinical, 37, 103289.

[19] Mekbib, D. B., Han, J., Zhang, L., Fang, S., Jiang, H., Zhu, J., ... & Xu, D. (2020). Virtual reality therapy for upper limb rehabilitation in patients with stroke: a meta-analysis of randomized clinical trials. Brain injury, 34(4), 456-465.

[20] Choi, J., Kim, K. T., Lee, J., Lee, S. J., & Kim, H. (2020, February). Robust semi-synchronous bci controller for brain-actuated exoskeleton system. In 2020 8th international winter conference on brain-computer interface (BCI) (pp. 1-3). IEEE.